# Half-metallic interface and coherent tunneling in $Co_2YZ/MgO/Co_2YZ$ ($YZ$=MnSi,CrAl) magnetic tunnel junctions: A first-principles study

Yoshio Miura, Hirohisa Uchida, Yoshihiro Oba, Kazutaka Abe, and Masafumi Shirai
*Research Institute of Electrical Communication, Tohoku University, Katahira 2-1-1, Aoba-ku, Sendai 980-8577, Japan*
(Received 31 May 2008; revised manuscript received 16 July 2008; published 18 August 2008)

We present first-principles based calculations of electronic structures and tunneling conductance of $Co_2YZ/MgO(\sim 2\ nm)/Co_2YZ(001)$ ($YZ$=MnSi,CrAl) magnetic tunnel junctions (MTJs). It is found that $YZ$(MnSi and CrAl)-terminated interfaces are thermodynamically stable as compared with Co-terminated interfaces in $Co_2YZ/MgO(001)$ junctions. In the CrAl-termination, no interface states appear in both sides of the junctions, preserving the half metallicity of $Co_2CrAl$, while reduction of the spin polarization is significant in the MnSi termination. $Co_2CrAl$, however, has no $\Delta_1$ band at the Fermi level, thus the majority-spin conductance of $Co_2CrAl/MgO/Co_2CrAl(001)$ MTJs in the parallel magnetization is much smaller than that of $Co_2MnSi/MgO/Co_2MnSi(001)$ MTJs. We propose that MTJs having an ultrathin $Co_2CrAl$ layer between $Co_2MnSi$ electrode and MgO barrier, i.e., $Co_2MnSi/Co_2CrAl/MgO(001)$ junctions, can derive both the half-metallic character at the interface and the large tunneling conductance through the $\Delta_1$ channel in the parallel magnetization.

DOI: 10.1103/PhysRevB.78.064416 PACS number(s): 73.20.At, 73.40.Rw, 85.75.Mm

## I. INTRODUCTION

The spin-dependent tunneling between ferromagnetic electrodes separated by insulating barriers provides the tunneling magnetoresistance (TMR) depending on relative magnetization directions of the two ferromagnetic electrodes.[1,2] The effect is essential for applications of spintronics such as the magnetoresistive random access memory (MRAM) and the read-out head of hard disk drives. The half-metallic ferromagnets (HMFs), which are metallic for the majority-spin state and semiconducting with an energy gap for the minority-spin state, leading to complete (100%) spin polarization at the Fermi level are one of key materials in obtaining huge TMR.

Among the many theoretically predicted HMFs,[3–9] the Co-based full Heusler alloys are the most promising candidates for use in spintronics devices owing to their high Curie temperatures above room temperature[10] (RT) and robustness of high spin polarization against atomic disorder.[11,12] Many experiments have been conducted on TMR measurements for MTJs with an amorphous alumina ($AlO_x$) barrier and Co-based full Heusler alloys, e.g., $Co_2(Cr_{0.6}Fe_{0.4})Al$,[13] $Co_2MnAl$,[14] $Co_2FeAl$,[15] $Co_2MnSi$,[16] and $Co_2Fe(Al_{0.5}Si_{0.5})$.[17] In particular, a large TMR ratio of 570% has been observed at 2 K for the $Co_2MnSi/AlO_x/Co_2MnSi$ MTJ.[16] It confirms the high spin polarization of $Co_2MnSi$ experimentally for the first time. However, the TMR ratio decreases rapidly with increasing temperature and reaches 67% at RT.

Recently, TMR ratio as high as 6000% was predicted in the Fe/MgO/Fe(001) MTJ from a ballistic conductance calculations.[18,19] It was found that the decay of the wave function with $\Delta_1$ symmetry is very slow as compared with that of $\Delta_2$ and $\Delta_5$ channels in the single crystalline MgO barrier owing to the symmetry compatibility with the complex $\Delta_1$ band in the insulating gap of the MgO. Since bcc-Fe is half metallic on the $\Delta_1$ band, the Fe/MgO/Fe(001) MTJ can provide very large TMR. In fact, high TMR ratios of about 180% for the Fe/MgO/Fe(001) MTJ (Ref. 20) and about 220% for CoFe/MgO/CoFe(001) MTJ (Ref. 21) have been obtained at RT. Furthermore, the TMR ratio was raised to 500% at RT for the MTJ with CoFeB electrodes and a MgO barrier.[22]

While the Fe/MgO/Fe(001) MTJ and related systems have succeeded in obtaining very large TMR ratio at RT, lower resistance has been required to achieve ultrahigh speed and high density in future spintronics applications. To this end, one needs a tunneling junction with a thin MgO barrier. However, the TMR ratio of Fe/MgO/Fe(001) and related systems rapidly decreases with the decreasing MgO barrier thickness owing to the contribution of the minority-spin $\Delta_5$ and $\Delta_2$ channels to the tunneling conductance through a thin MgO barrier. The use of the HMF as an electrode in the MTJ with MgO barrier (HMF/MgO/HMF) can be expected to suppress the tunneling from the minority-spin $\Delta_5$ and $\Delta_2$ states in such a thin MgO barrier and has a potential to overcome this problem.

The MTJs composed of the MgO barrier and half-metallic Co-based full Heusler alloys, e.g., $Co_2Fe(Al_{0.5}Si_{0.5})$,[23] $Co_2(Cr_{0.6}Fe_{0.4})Al$,[24] and $Co_2MnSi$,[25] were fabricated in recent years, and the TMR ratio has been improved steadily. However, the TMR ratio still depends on temperature considerably because the tunneling conductance in the antiparallel magnetization increases with increasing temperature. For example, high TMR ratio of 683% observed at 4.2 K for the $Co_2MnSi/MgO/Co_2MnSi$ MTJ (Ref. 25) decreases to 179% at RT. It is considered that the thermal fluctuation of magnetic spin moments[26] of the HMF electrodes causes incoherent or nonquasiparticle states in the minority-spin gap and gives rise to the reduction of the spin polarization and considerable contributions to the tunneling conductance of MTJs in the antiparallel magnetization.[27] Furthermore, Mavropoulos *et al.*[28] suggested that interface states appeared in the minority-spin gap at the junctions of MTJs can also contribute to the tunneling conductance in the antiparallel magnetization through spin mixing processes such as magnon excitations and inelastic scattering at RT.

 

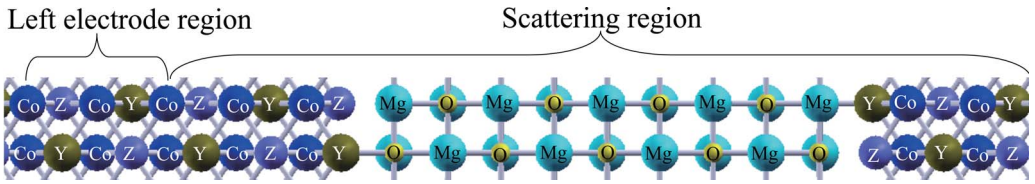


FIG. 1. (Color online) A supercell of the $Co_2YZ/MgO/Co_2YZ$ ($YZ$=MnSi or CrAl) MTJ with $YZ$ termination and corresponding left electrode and scattering regions assumed in conductance calculations (see text).

In this paper, we perform first-principles electronic structure calculations and ballistic conductance calculations in order to clarify electronic and transport properties of MTJs with $Co_2YZ$ ($YZ$=MnSi,CrAl) and MgO barriers. First, we carefully determine stable interfacial structures at $Co_2YZ/MgO(001)$ junctions. We will show that $YZ$(MnSi and CrAl)-terminated interfaces are thermodynamically stable as compared with Co-terminated interfaces. In particular, we find that the CrAl-terminated $Co_2CrAl/MgO(001)$ interface is half metallic without any interface states in both sides of the junctions, while the MnSi-terminated $Co_2MnSi/MgO(001)$ interface looses the half metallicity of $Co_2MnSi$. The half-metallic character at interfaces is important to suppress the tunneling conductance through interface states in the antiparallel magnetization. Then, we will show that the majority-spin conductance of $Co_2CrAl/MgO/Co_2CrAl$ (001) MTJs in the parallel magnetization is much smaller than that of $Co_2MnSi/MgO/Co_2MnSi$ (001) MTJs owing to the absence of the $\Delta_1$ band around the Fermi level in $Co_2CrAl$. It is considered that the $\Delta_1$ band in the majority-spin state is also essential to obtain a large TMR ratio for MgO-based MTJs. Here, we propose that addition of an ultrathin $Co_2CrAl$ layer between $Co_2MnSi$ electrode and MgO barrier can eliminate interface states while preserving the coherent tunneling through the $\Delta_1$ band of the MTJ in the parallel magnetization.

## II. COMPUTATIONAL METHOD

We perform first-principles calculations for supercells consisting of $Co_2YZ$ ($YZ$=MnSi or CrAl) and MgO using the density-functional theory within the generalized-gradient approximation for the exchange-correlation energy.[29] In order to facilitate the structure optimization, which is important for determining the interface structure, we adopt plane-wave basis sets along with the ultrasoft pseudopotential method by using the quantum code ESPRESSO.[30] The number of **k** points is taken to be $10\times10\times1$ for all cases, and Methfessel-Paxton smearing with a broadening parameter of 0.01 Ry is used. The cutoff energy for the wave function and charge density is set to 30 and 300 Ry, respectively. These values are large enough to deal with all the elements considered here within the ultrasoft pseudopotential method.

A $Co_2YZ/MgO/Co_2YZ(001)$ MTJ is constructed in a tetragonal supercell, where the in-plane lattice parameter of the supercell is fixed at 3.99 and 4.05 Å for $YZ$=MnSi and CrAl, respectively. These values correspond to $a_0/\sqrt{2}$, where $a_0$ is the lattice constant of the bulk $Co_2MnSi$(5.65 Å) and $Co_2CrAl$(5.73 Å). Since the lattice constant of the rock salt MgO is 4.21 Å, the lattice mismatches between $Co_2YZ$ and MgO on the 45° in-plane rotation at (001) face are 5.1% for $Co_2MnSi$ and 3.8% for $Co_2CrAl$, which lead to 11.2% and 8.3% of tetragonal expansions along longitudinal ($z$ axis) direction in MgO, respectively. The $Co_2YZ/MgO(001)$ interface has two types of termination on $Co_2YZ$, namely, the Co termination and the $YZ$ termination. We prepare the supercell of multilayer containing nine atomic layers of MgO and 17 and 15 atomic layers of $Co_2YZ$ for the Co- and $YZ$-terminated interfaces, respectively. Figure 1 schematizes the supercell of the $Co_2YZ/MgO(9)/Co_2YZ(001)$ MTJ for the $YZ$ termination. The supercell of the Co termination has two more Co atoms at both sides of the MgO junctions in the supercell of the $YZ$ termination.

For conductance calculations, we consider an open quantum system consisting of a scattering region corresponding to MgO and a junction with $Co_2YZ$ attached to left and right semi-infinite electrodes corresponding to bulk $Co_2YZ$. Conductance is obtained by solving the scattering equation with infinite boundary conditions in which the wave function of the scattering region and its derivative are connected to the Bloch states of each electrode.[31] The potential in the scattering equation can be obtained from the self-consistent electronic structure calculations for the supercell containing a left and a scattering region. Corresponding left electrode and scattering region used in the conductance calculations are shown in Fig. 1. We confirmed that five atomic layers of $Co_2YZ$ between the right edge of the electrode region and the left-hand side of the $Co_2YZ/MgO$ interface are enough to represent the shape of the local potential of bulk $Co_2YZ$ in the electrode region.

Since our system is repeated periodically in the $xy$ plane and propagating states can be assigned by an in-plane wave vector $k_\parallel=(k_x,k_y)$ index, different $k_\parallel$ do not mix and can be treated separately. Furthermore, our approach neglects the spin-orbit interaction and noncollinear spin configuration. Thus, we solve scattering equations for some fixed $k_\parallel$ and spin index on the basis of approaches of Choi and Ihm.[31,32]

## III. RESULTS AND DISCUSSION

### A. Interfacial structure of $Co_2YZ/MgO(001)$

The $Co_2YZ/MgO(001)$ junction has three possible configurations for each termination where atoms terminating $Co_2YZ$ are positioned: on top of the O atoms (O-top), Mg atoms (Mg-top), or hollow of the MgO(001) surface. In order to determine the stable interfacial configuration for each termination in $Co_2YZ/MgO(001)$ junctions, we minimized the

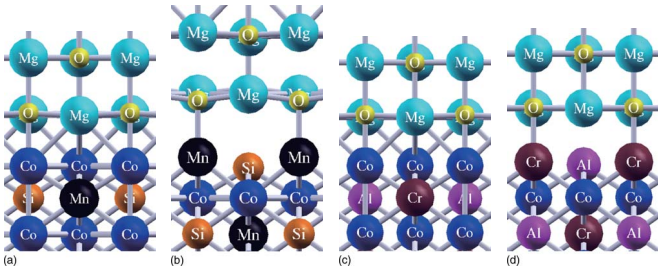


FIG. 2. (Color online) Magnifications of the cross-sectional view of (a) Co- and (b) MnSi-terminated $Co_2MnSi/MgO(001)$ interface and (c) Co- and (d) CrAl-terminated $Co_2CrAl/MgO(001)$ interfaces with the O-top configuration, where atoms terminating $Co_2YZ$ are positioned on top of the O atoms in the MgO(001) surface. The atomic position is determined so as to minimize the total energy of each termination.

total energy by relaxing atomic positions except for atoms in the electrode region with changing the longitudinal size of the supercell. We found that the O-top configuration is most stable among the other configurations (Mg-top and hollow) owing to the hybridization between $3d_{3z^2-r^2}$ orbital of the transition atoms (Co, Mn, and Cr) and $p_z$ orbital of O atom. The magnifications of the $Co_2YZ/MgO(001)$ interfacial structure with O-top configuration are schematized in Fig. 2 for each termination, which shows how the interfacial atoms move after the relaxations.

As can be seen in Figs. 2(a) and 2(c), the Co-terminated interface has a simple structure with 2.0 Å of interfacial distance both for the $Co_2MnSi/MgO(001)$ and $Co_2CrAl/MgO(001)$ junctions. On the other hand, structures of the *YZ*-terminated interface are a little bit complicated. For instance, in the case of the MnSi termination, the Mn-O distance is 2.25 Å, while the Si-O distance is 3.17 Å. This can be attributed to the difference in the covalent bond radii of Mn and Si atoms. Since the covalent bond radius of the Si atom (1.11 Å) is smaller than that of the Mn atom (1.39 Å), the interfacial Si atom of the MnSi termination cannot keep the Co-Si distance of the bulk $Co_2MnSi$ (2.42 Å). Consequently, the Si atom moves toward the Co atom side and only the Mn atom makes a bond with the O atom. In fact, the Co-Si distance (2.33 Å) of the MnSi termination corresponds to that of the bulk $CoSi_2$ with Fluorite (C1) structure (2.32 Å). Similar structure is observed in the CrAl-terminated interface because of the difference in the covalent bond radius of Cr (1.27 Å) and Al atoms (1.18 Å), while the Cr-O and Al-O distances (2.20 and 2.34 Å) are smaller than those of the MnSi-terminated interface.

The relative stability between the Co- and *YZ*-terminated interfaces is given by the formation energy

$$E_{\text{form}}^{\text{term}} = E_{\text{tot}}^{\text{term}} - \sum_i N_i \mu_i, \tag{1}$$

where $E_{\text{tot}}^{\text{term}}$ is the total energy of the supercell for each termination, $N_i$ the number of atoms of each element, and $\mu_i$ their chemical potentials. At equilibrium, the chemical potential of the constituent atoms cannot exceed the corresponding one of the bulk phase, i.e., upper limit of $\mu_i$ can be derived from the bulk total energy per atom. Here, $\mu_{\text{Co(bulk)}}$ is taken from hcp-Co, $\mu_{\text{Mn(bulk)}}$ and $\mu_{\text{Cr(bulk)}}$ from antiferromagnetic $\alpha$-Mn and bcc-Cr, and $\mu_{\text{Si(bulk)}}$ and $\mu_{\text{Al(bulk)}}$ from diamond structure Si and fcc-Al, respectively. Since each supercell is nonstoichiometric only on Co atom, the difference of the formation energy between Co and *YZ* termination $E_{\text{form}}^{\text{diff}} = (E_{\text{form}}^{\text{Co term}} - E_{\text{form}}^{YZ\ \text{term}})/2$ can be expressed as function of $\mu_{\text{Co}}$ only. Furthermore, assuming the thermodynamic equilibrium condition $\mu_{Co_2YZ} = 2\ \mu_{\text{Co}} + \mu_Y + \mu_Z$ and taking $\mu_{Co_2YZ}$ from the bulk structure, we can determine the lower limit of $\mu_{\text{Co}}$ as $\mu_{\text{Co}} \geq \mu_{Co_2YZ} - \mu_{Y(\text{bulk})} - \mu_{Z(\text{bulk})}$, i.e., the formation energy difference is expressed within the thermodynamically allowed range $\mu_{Co_2YZ} - \mu_{Y(\text{bulk})} - \mu_{Z(\text{bulk})} \leq \mu_{\text{Co}} \leq \mu_{\text{Co(bulk)}}$. It is conventional to refer to the upper limit of $\mu_{\text{Co}}$ as the Co-rich limit and to the lower limit as the Co-poor limit.

TABLE I. The formation energy difference between the Co- and *YZ*-terminated interfaces $E_{\text{form}}^{\text{diff}}$ for the Co-rich and Co-poor limits. The positive (negative) value of $E_{\text{form}}^{\text{diff}}$ indicates that the *YZ*-terminated interface is more (less) stable than the Co-terminated interface. $\mu_{\text{Co(rich)}} - \mu_{\text{Co(poor)}}$ means the difference of the chemical potential between the Co-rich and Co-poor limits (see text).

| (eV) | $Co_2MnSi/MgO$ | $Co_2CrAl/MgO$ |
|---|---|---|
| $\mu_{\text{Co(rich)}} - \mu_{\text{Co(poor)}}$ | 0.967 | 0.455 |
| $E_{\text{form}}^{\text{diff}}$(Co-poor) | 1.91 | 1.19 |
| $E_{\text{form}}^{\text{diff}}$(Co-rich) | −0.0249 | 0.282 |

Table I shows the $E_{\text{form}}^{\text{diff}}$ for the $Co_2MnSi/MgO(001)$ and $Co_2CrAl/MgO(001)$ junctions with the O-top configuration for the Co-rich and Co-poor limits. The positive (negative) value of $E_{\text{form}}^{\text{diff}}$ indicates that the *YZ*-terminated interface is more (less) stable than the Co-terminated interface. In the Co-rich case of the $Co_2MnSi/MgO(001)$, the Co termination is slightly stable as compared with the MnSi termination. However, in the wide range of the $\mu_{\text{Co}}$, the MnSi termination is more favorable than the Co termination. Furthermore, in the case of the $Co_2CrAl/MgO(001)$, the CrAl termination is more stable than the Co termination irrespective of the $\mu_{\text{Co}}$. We consider that the relaxations of atomic positions in the *YZ*-terminated interfaces significantly reduce the formation energy of the supercell. These results are consistent with the formation energy calculations for the $Co_2MnSi(001)$ *surface*, where the MnSi-terminated surface is more stable than the Co-terminated surface.[33]

In our previous study,[34] we adopted the Co termination as an interfacial structure of the $Co_2MnSi/MgO(001)$ junction because of its large adhesion energy as compared with that of the MnSi termination. In experiments, the $Co_2YZ$ film is annealed after deposition on a buffer layer in order to obtain ordered $L2_1$ structures. This means that a thermodynamically stable structure, i.e., the *YZ*-terminated interface will appear in the $Co_2YZ/MgO$ junction. Thus, in this paper, we focus on the *YZ*-terminated interface of the $Co_2YZ/MgO(001)$ junction and discuss its electronic structures and transport properties.

### B. Electronic structure of $Co_2YZ/MgO(001)$

Figure 3 shows majority- and minority-spin local density of states (LDOSs) at the Fermi level projected on to each

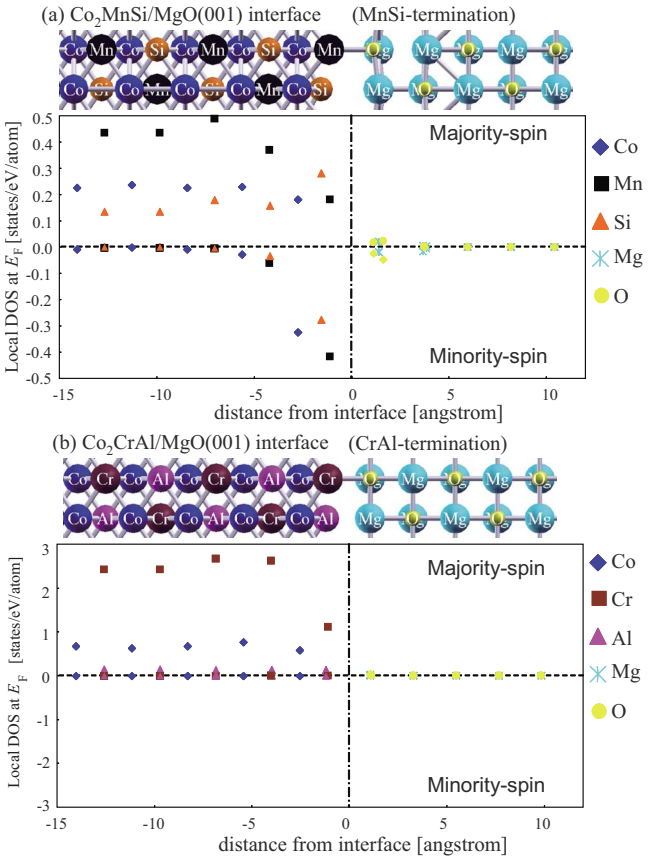


FIG. 3. (Color online) The local density of states (LDOSs) at the Fermi level projected on to each atomic sphere as a function of the distance from interface for (a) $Co_2MnSi/MgO(001)$ and (b) $Co_2CrAl/MgO(001)$ junctions, respectively. The positive (negative) sign of $y$ axis indicates majority-spin (minority-spin) LDOS. Schematic figures of the supercell of the $Co_2YZ/MgO/Co_2YZ(001)$ MTJ are shown above the LDOS, respectively.

atomic sphere as a function of the distance from the $Co_2YZ/MgO(001)$ junction. It is found that in the case of the MnSi termination, interface states appear in the minority-spin state at the Fermi level, reducing the half metallicity of the $Co_2MnSi$. Similar results have been obtained in the Co termination of the $Co_2MnSi/MgO(001)$ junction.[34] In contrast, the CrAl termination has no interface states in the minority-spin state at the Fermi level in both sides of the junctions.

To see electronic structures at interface in more detail, we present in Figs. 4 and 5 the majority- and minority-spin LDOSs of each atom and atomic orbital in the $YZ$-terminated $Co_2YZ/MgO(001)$ interface. The LDOSs in the bulk (electrode) region are also shown as a reference. In Figs. 4(a) and 4(b), minority-spin states are observed around the Fermi level in the LDOSs of the interfacial Mn and Si atoms. The spin polarizations of interfacial Mn and Si are −40% and 1.0%, respectively. At the interface, the Mn atom looses half of its first neighbor Co atoms, and nonbonding Mn $3d$ states (possibly $d_{yz}$, $d_{zx}$, and $d_{3z^2-r^2}$) can appear around the Fermi level. Since the Mn $3d_{3z^2-r^2}$ orbital hybridizes with the O $2p_z$ orbital at the interface, the LDOSs of the interfacial Mn $3d_\gamma$ states keep half-metallic character. Contrary to this, interfacial Mn $3d_\epsilon$ orbital ($3d_{yz}$ and $3d_{zx}$) becomes nonbonding in the O-top configuration, reducing the spin polarization at the MnSi-terminated interface.

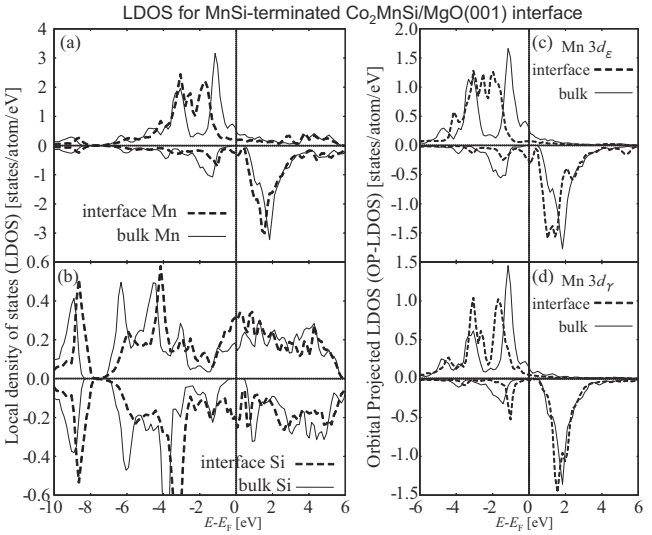


FIG. 4. Dashed lines show the local density of states of (a) Mn, (b) Si, (c) Mn $3d_\epsilon$, and (d) Mn $3d_\gamma$ at the MnSi-terminated $Co_2MnSi/MgO(001)$ interface as a function of energy relative to the Fermi energy. The LDOSs in the bulk (electrode) region are also shown as a reference by solid line in each figure. The sign of LDOS indicates the majority-spin (positive) and minority-spin (negative) states.

In Fig. 5, on the other hand, the LDOSs of the interfacial Cr and Al show the clear minority-spin gap, and the half-metallic character of $Co_2CrAl$ is preserved at the CrAl terminated interface. It is important to refer that the (100) CrAl-terminated surface was previously predicted to have a high

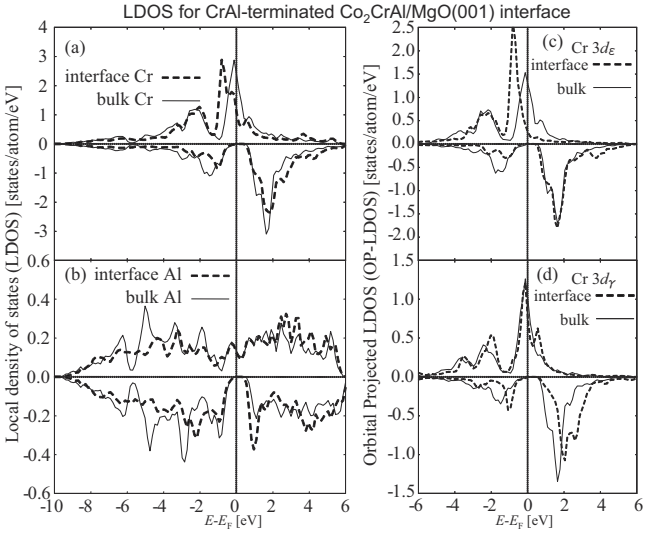


FIG. 5. Dashed lines show the local density of states of (a) Cr, (b) Al, (c) Cr $3d_\epsilon$, and (d) Cr $3d_\gamma$ at the CrAl-terminated $Co_2CrAl/MgO(001)$ interface as a function of energy relative to the Fermi energy. The LDOSs in the bulk (electrode) region are also shown as a reference by solid line in each figure. The sign of LDOS indicates the majority-spin (positive) and minority-spin (negative) states.

TABLE II. The local magnetization ($\mu_B$) at the interface and bulk regions of the *YZ*-terminated $Co_2YZ$/MgO(001) junctions (*YZ*=MnSi,CrAl).

| ($\mu_B$) | | | | |
|---|---|---|---|---|
| $Co_2MnSi$/MgO(001) | Co | Mn | Si | O |
| Interfacial region | 0.936 | 4.06 | −0.185 | −0.0342 |
| Bulk region | 0.935 | 3.31 | −0.115 | 0.00 |
| $Co_2CrAl$/MgO(001) | Co | Cr | Al | O |
| Interfacial region | 0.832 | 3.10 | −0.121 | 0.0110 |
| Bulk region | 0.712 | 1.78 | −0.161 | 0.00 |

spin polarization of about 85%,[35] while the spin polarization is degraded significantly at the CrAl-terminated $Co_2CrAl$/GaAs(100) interface.[36] Since the GaAs has narrow gap around the Fermi level as compared with the MgO, the half-metallic character of the CrAl-terminated surface is destroyed significantly once the surface is attached by GaAs.

Table II lists the local spin moments of Co, *Y* (Mn or Cr), *Z* (Si or Al), and O atoms at the interfacial region and in the bulk region. It is found that the spin moments of the interfacial Mn (4.06 $\mu_B$) and Cr (3.10 $\mu_B$) are larger than those of the bulk $Co_2MnSi$ (3.31 $\mu_B$) and $Co_2CrAl$ (1.78 $\mu_B$) because of the charge transfer from the minority-spin to the majority-spin states. We consider that the relaxation of the atomic positions and the reduced symmetry at the interface cause charge transfer from the minority-spin to the majority-spin 3*d* states owing to the localization effect of 3*d* electrons.

We should discuss why the CrAl termination is half metallic while the MnSi termination is not. In the case of $Co_2MnSi$, the majority-spin Mn $3d_\epsilon$ states are nearly occupied [see Fig. 3(c)]. This suppresses the charge transfer in the interfacial region and leaves electrons in the nonbonding $3d_\epsilon$ states in the minority-spin gap, leading to the reduction of the spin polarization at the interface. On the other hand, in the case of $Co_2CrAl$, the majority-spin Cr $3d_\epsilon$ states are partially occupied [see Fig. 3(c), and a large amount of minority-spin charge can transfer to the majority-spin states in the interfacial region. The charge transfer diminishes electrons in the nonbonding minority-spin Cr $3d_\epsilon$ states and acts to reconstruct the half-metallic gap in the LDOS of the interfacial Cr atom. In fact, the local spin moment of Cr in the CrAl-terminated interface is increased by 1.35 $\mu_B$ from the bulk one, which is larger than that of Mn atom in the MnSi-terminated interface (increased by 0.75 $\mu_B$ from the bulk one). The large enhancement of the Cr spin moment is observed also in the CrAl-terminated surface.[35] It is considered that the large enhancement of the interfacial Cr spin moment is a result of the large amount of charge transfer from the minority-spin to the majority-spin Cr $3d_\epsilon$ states, leading to the half-metallic character of the CrAl termination.

### C. Transport properties of $Co_2YZ$/MgO/$Co_2YZ$

We show in Fig. 6 the energy dependence of the transmittance at $k_\parallel=(0,0)$ for the $Co_2MnSi$/MgO(9)/$Co_2MnSi$(001) MTJ (CMS/MgO/CMS) and the $Co_2CrAl$/MgO(9)/$Co_2CrAl$(001) MTJ (CCA/MgO/CCA), respectively. The band structures of bulk $Co_2MnSi$ and $Co_2CrAl$ along the [001] direction at $k_\parallel=(0,0)$ are presented for comparison. Note that these results show the zero-bias conductance at each energy and do not indicate the bias volt-

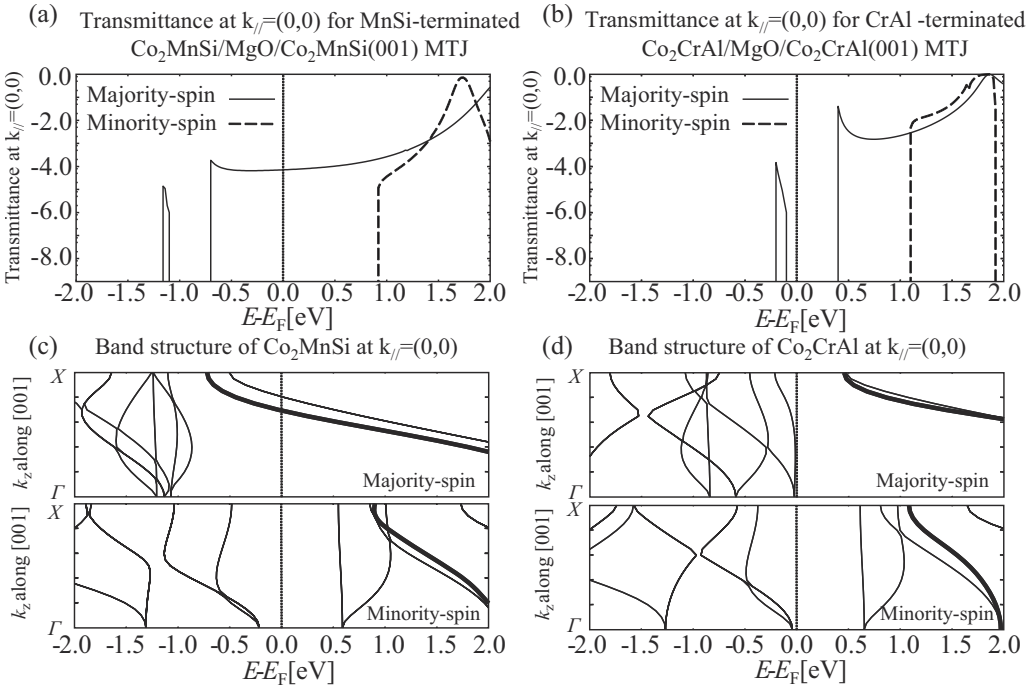


FIG. 6. The majority- and minority-spin transmittances as a function of energy at $k_\parallel=(0,0)$ for (a) $Co_2MnSi$/MgO(9)/$Co_2MnSi$ (001) and (b) $Co_2CrAl$/MgO(9)/$Co_2CrAl$ (001) MTJs in the parallel magnetization. The majority- and minority-spin band structures of bulk (c) $Co_2MnSi$ and (d) $Co_2CrAl$ along [001] direction at $k_\parallel=(0,0)$ are also shown, where bold lines indicate the conduction band with $\Delta_1$ symmetry. The scale of the vertical axis for transmittance is logarithmic.

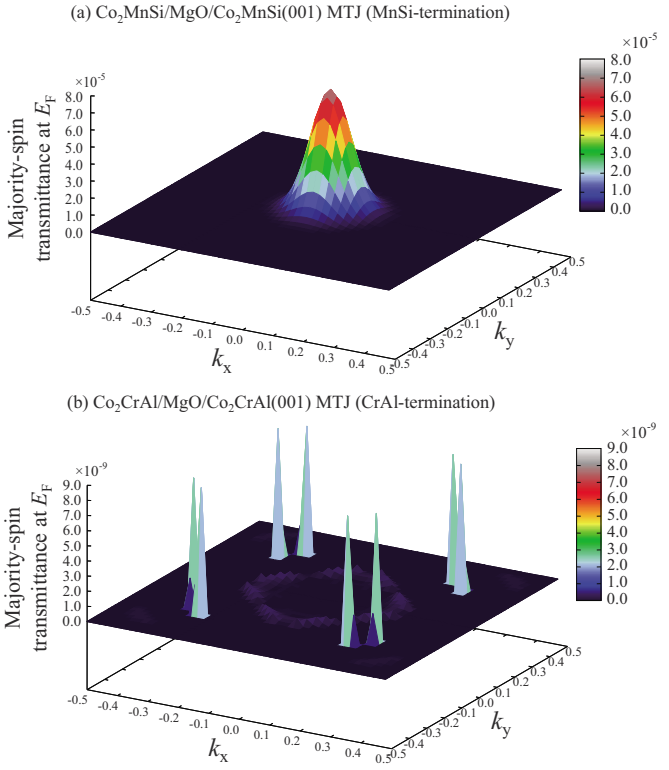


FIG. 7. (Color online) In-plane wave vector $k_{\|}=(k_x,k_y)$ dependence of majority-spin transmittance at the Fermi level for (a) $Co_2MnSi/MgO(9)/Co_2MnSi(001)$ and (b) $Co_2CrAl/MgO(9)/Co_2CrAl(001)$ MTJs in the parallel magnetization.

age dependence of conductance. It is found in both cases that the transmittance increases with increasing energy, and the thresholds coincide with the bottom of the broad conduction bands of bulk $Co_2MnSi$ and $Co_2CrAl$. This means that the conduction bands are the main contributing factor to the transmittance at $k_{\|}=(0,0)$.

From the symmetry analysis of the $Co_2MnSi$ band structure, we found that the majority-spin conduction band on the lower energy side [shown by bold solid line in Fig. 6(c)] has the $\Delta_1$ symmetry. Furthermore, the majority-spin conduction band on the higher energy side is doubly degenerate and has the $\Delta_5$ symmetry. Similarly, the unoccupied conduction band in the majority-spin state on the lower energy side of bulk $Co_2CrAl$ [shown by bold solid line in Fig. 6(d)] has the $\Delta_1$ symmetry, and the doubly degenerate conduction bands have the $\Delta_5$ symmetry. We have confirmed that the conduction band with $\Delta_1$ symmetry dominated the tunneling and that the transmittance from the $\Delta_1$ band was three orders of magnitude larger than that from the $\Delta_5$ band owing to the symmetry compatibility with MgO complex bands within the energy gap. Similar to this, the majority-spin band across the Fermi level of bulk $Co_2CrAl$ has $\Delta_2$ symmetry, and the wave function shows a rapid decay in the MgO barrier.

Figures 7(a) and 7(b) plot the majority-spin transmittance at the Fermi level for the CMS/MgO/CMS and CCA/MgO/CCA, respectively, as a function of the in-plane wave vector $k_{\|}=(k_x,k_y)$. A peak centered at $k_{\|}=(0,0)$ is found in the $k_{\|}$ dependence of the CMS/MgO/CMS owing to the coherent tunneling through the $\Delta_1$ channel. On the other hand, the transmittance for the CCA/MgO/CCA has no peak at $k_{\|}=(0,0)$ and shows spiky structures in the two-dimensional (2D) Brillouin zone, which was so-called *hot spot* conductance and attributed to the resonant tunneling between the interface states.[37] The averaged conductance over the 2D Brillouin zone for the CCA/MgO/CCA is about $5.55\times10^{-11}G_0$, which is much smaller than $1.55\times10^{-6}G_0$ for the CMS/MgO/CMS, where $G_0$ is $e^2/h$ unit. This large difference in the $k_{\|}$ dependence of the transmittance can be understood by considering the majority-spin band structures of the $Co_2MnSi$ and $Co_2CrAl$ around the Fermi level.

In bulk $Co_2YZ$ ($YZ$=MnSi and CrAl), the $\Delta_1$ band is unoccupied or partially occupied depending on the number of valence electrons of $Co_2YZ$. This can be understood in terms of the well-known Slater-Pauling behavior of the total magnetization $M_t=Z_v-24$, where $Z_v$ is the number of valence electrons and 24 means 12 occupied states per spin in $Co_2YZ$.[8] In this picture, the occupancy of the minority-spin bands of $Co_2YZ$ does not change and the extra electrons depending on $Y$ and $Z$ atoms fill the majority-spin bands only. Since $Co_2MnSi(Z_v=29)$ has two additional valence electrons as compared with $Co_2CrAl(Z_v=27)$, the Fermi level shifts to higher energies with increasing $Z_v$ in the majority-spin state. As a result, the majority-spin $\Delta_1$ band is partially occupied for $Co_2MnSi$ and unoccupied for $Co_2CrAl$. From the chemical trend in the majority-spin band dispersions of Co-based full Heusler alloys, the position of the Fermi level is classified by $Z_v$ as follows: the Fermi level crosses the $\Delta_1$ bands for $Z_v\geq28.0$, while it is positioned around the localized $d$ bands with the $\Delta_2$ symmetry for $Z_v<28.0$. Thus, it can be concluded that $Co_2MnAl(Z_v=28)$, $Co_2MnSi(Z_v=29)$, $Co_2MnGe(Z_v=29)$, $Co_2FeAl(Z_v=29)$, $Co_2Fe(Al_{0.5}Si_{0.5})$ ($Z_v=29.5$), and $Co_2FeSi(Z_v=30)$ will show coherent tunneling through the $\Delta_1$ channel in the parallel magnetization, while $Co_2VAl(Z_v=26)$, $Co_2VGa(Z_v=26)$, $Co_2CrAl(Z_v=27)$, and $Co_2CrGa(Z_v=27)$ show *hot-spot* tunneling in MgO-based MTJs even in the parallel magnetization.

Then, we discuss the minority-spin transmittance of the MTJs. The dashed lines in Figs. 6(a) and 6(b) show the minority-spin transmittance at $k_{\|}=(0,0)$ for the CMS/MgO/CMS and CCA/MgO/CCA. It is found that the minority-spin transmittance around the Fermi energy becomes zero because of the half-metallic character of bulk $Co_2MnSi$ and $Co_2CrAl$. In addition, the threshold energy of the transmittance at $k_{\|}=(0,0)$ ($\sim1$ eV) is larger than the conduction-band edge ($\sim0.5$ eV above the Fermi level) in the DOS of the bulk $Co_2YZ$(see Figs. 4 and 5). This is an advantage of MTJs with MgO barrier over MTJs with Al-O barrier because in the latter, all channels in the minority-spin state can contribute equally to the transmittance and degrade the TMR.

### D. Electronic and transport properties of $Co_2MnSi/(Co_2CrAl)_1/MgO/(Co_2CrAl)_1/Co_2MnSi$

Recent experiments on the TMR measurements for the MTJs with MgO and Co-based full Heusler alloys show rela-

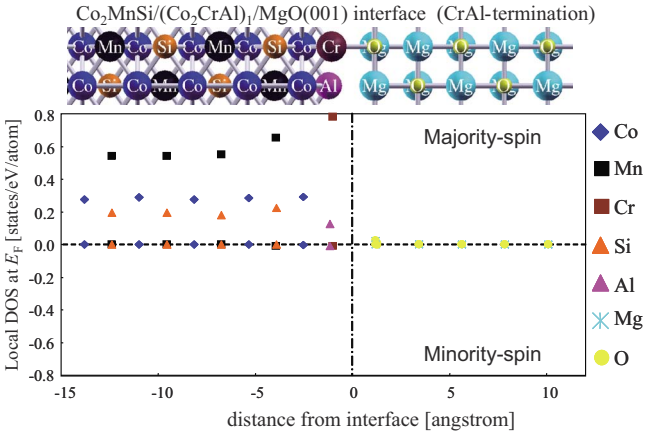


FIG. 8. (Color online) The local density of states at the Fermi level projected on to each atomic sphere as a function of the distance along [001] for the $Co_2MnSi/(Co_2CrAl)_1/MgO(001)$ junction. The positive (negative) sign of $y$ axis indicates majority-spin (minority-spin) LDOS. A schematic figure of the $Co_2MnSi/(Co_2CrAl)_1/MgO/(001)$ junction is shown above the LDOS.

tively large TMR ratio at low temperature.[23–25] However, the tunneling conductance in the antiparallel magnetization increases with increasing temperature, leading to the significant reduction of the TMR ratio at RT in the MTJs. Mavropoulos *et al.*[28] have pointed out that spin mixing process, such as magnon excitations and inelastic scattering through interface states, is one possible reason for the tunneling conductance in the antiparallel magnetization at RT. We consider that the half-metallic character of the $Co_2CrAl/MgO(001)$ interface presented in this work will be effective to suppress the tunneling conductance through interface states in the antiparallel magnetization. However, the $Co_2CrAl/MgO/Co_2CrAl(001)$ MTJ shows considerably small tunneling conductance in the parallel magnetization owing to the absence of the $\Delta_1$ band around the Fermi level in the $Co_2CrAl$. The presence of the $\Delta_1$ band in the majority-spin state is also essential to obtain a large tunneling conductance in the parallel magnetization for the MgO-based MTJs. In addition, it is reported that the bulk $Co_2CrAl$ is thermodynamically unstable resulting in the phase separation at RT.[38] Thus, the $Co_2CrAl$ is unfavorable as an electrode of the MgO-based MTJ.

In order to utilize the half-metallic character of the CrAl termination with preserving the coherent tunneling through the $\Delta_1$ channel, we inserted one monolayer of $Co_2CrAl$ between $Co_2MnSi$ electrode and MgO barrier. Figure 8 shows majority- and minority-spin LDOS at the Fermi level of the $Co_2MnSi/(Co_2CrAl)_1/MgO(001)$ junction projected on to each atomic sphere as a function of the distance from the interface. It is found that the junction has no interface states in the minority-spin states, i.e., one monolayer of $Co_2CrAl$ is enough to eliminate the interface states in the minority-spin gap. Furthermore, the LDOSs of the interfacial Cr, Mn, Si, and Al in Figs. 9(a) and 9(b) show clear gap in the minority-spin state, indicating the half-metallic behavior of the CrAl-terminated $Co_2MnSi/(Co_2CrAl)_1/MgO(001)$ interface.

Figure 10 shows the in-plane wave vector ($k_\parallel$) dependence

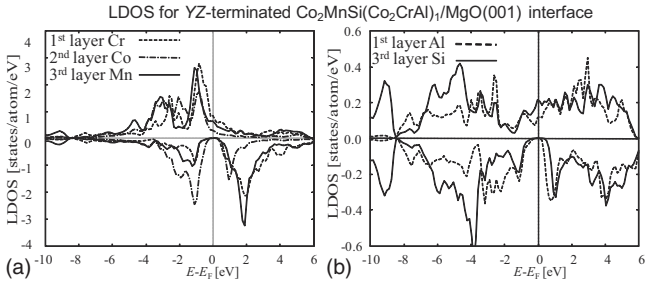


FIG. 9. (a) The local density of states of the first layer Cr (dashed lines), the second layer Co (long dashed dotted lines), and the third layer Mn (solid lines) from the $Co_2MnSi/(Co_2CrAl)_1/MgO(001)$ interface as a function of energy relative to the Fermi energy. (b) The LDOS of the first layer Al (dashed lines) and the third layer Si (solid lines) from the $Co_2MnSi/(Co_2CrAl)_1/MgO(001)$ interface as a function of energy relative to the Fermi energy. The sign of LDOS indicates the majority-spin (positive) and minority-spin (negative) states.

of the majority-spin transmittance at the Fermi level for the $Co_2MnSi/(Co_2CrAl)_1/MgO(9)/(Co_2CrAl)_1/Co_2MnSi$ (001) MTJ ($CMS/CCA_1/MgO/CCA_1/CMS$). We can find a broad peaked structure caving around $k_\parallel=(0,0)$. The caving structure around $k_\parallel=(0,0)$ indicates that the $Co_2CrAl$ adlayer decreases the transmittance through the $\Delta_1$ channel of the MTJ. The averaged conductance over 2D $k_\parallel$ is about $6.42\times10^{-8}G_0$, which is smaller than $1.55\times10^{-6}G_0$ for the CMS/MgO/CMS, but much larger than $5.55\times10^{-11}G_0$ for the CCA/MgO/CCA. Furthermore, we show in Fig. 11 that the energy dependence of the transmittance at $k_\parallel=(0,0)$ for the $CMS/CCA_1/MgO/CCA_1/CMS$. We can find an abrupt decrease in the majority-spin transmittance around $\sim-0.1$ eV which is due to fast decay of the wave function with the $\Delta_1$ symmetry at the $Co_2CrAl$ adlayer. However, the energy range with nonzero transmittance is almost the same with that of the $\Delta_1$ band of bulk $Co_2MnSi$ in both majority- and minority-spin states. These results suggest that a MTJ having $Co_2MnSi/(Co_2CrAl)_1/MgO$ junction can retain the coherent tunneling through the $\Delta_1$ channel in the parallel magnetization.

We have confirmed that the junction with two-monolayer $Co_2CrAl$ between $Co_2MnSi$ electrode and MgO barrier also

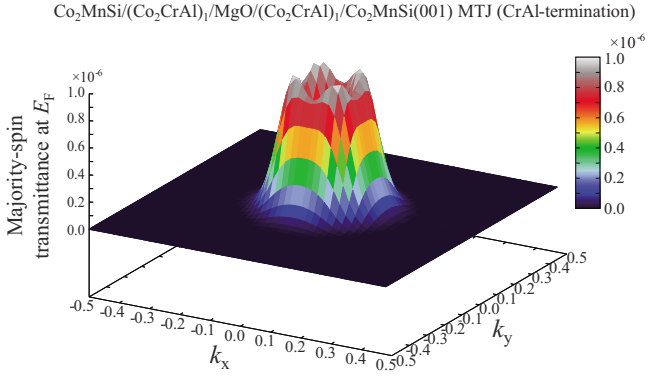


FIG. 10. (Color online) In-plane wave vector $k_\parallel=(k_x,k_y)$ dependence of majority-spin transmittance at the Fermi level for the $Co_2MnSi/(Co_2CrAl)_1/MgO(9)/(Co_2CrAl)_1/Co_2MnSi(001)$ MTJ in the parallel magnetization.

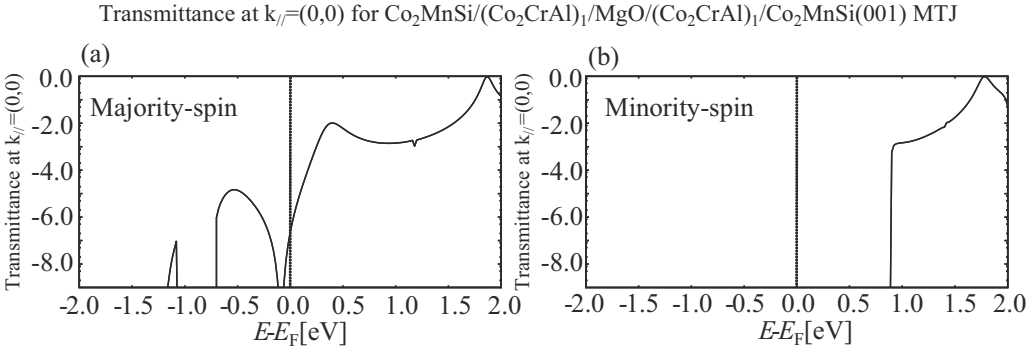


FIG. 11. Transmittance at $k_{\|}=(0,0)$ as a function of energy for $Co_2MnSi/(Co_2CrAl)_1/MgO(9)/(Co_2CrAl)_1/Co_2MnSi(001)$ MTJ in the parallel magnetization for the (a) majority- and (b) minority-spin channels, respectively. The scale of the vertical axis is logarithmic.

shows half-metallic character and retains the coherent tunneling through the $\Delta_1$ channel. Fabrication of half-metallic $Co_2MnSi/Co_2CrAl/MgO(001)$ junctions will be possible experimentally by depositing an ultrathin $Co_2CrAl$ layer on $Co_2MnSi$ electrode or MgO barrier. The half-metallic $Co_2MnSi/Co_2CrAl/MgO(001)$ junction will contribute to suppress the tunneling conductance in the antiparallel magnetization through interface states which are possible reasons for the large temperature dependence of TMR ratios observed in experiments. Our proposal will be effective also for spin injection into nonmagnetic semiconductors through MgO barrier such as $Co_2MnSi/MgO/GaAs(001)$.[39]

Finally, we generalize our results as follows: As mentioned in Sec. III B, the presence of partially occupied majority-spin $3d$ sates in $Co_2YZ$ plays an important role for the half-metallic character at interfaces with MgO. This means that other half-metallic $Co_2YZ$ having partially occupied $3d$ states such as $Co_2CrGa(Z_v=27)$ could be half metallic at the junction with MgO. Furthermore, the occupancy of $3d$ bands and $\Delta_1$ band in the majority-spin state of $Co_2YZ$ is characterized by the number of valence electrons. Thus, MTJs having an ultrathin $Co_2YZ(Z_v \approx 27)$ layer between MgO barrier and $Co_2YZ(Z_v \geq 28)$ electrode, i.e., $Co_2YZ(Z_v \geq 28)/Co_2YZ(Z_v \approx 27)/MgO(001)$ junctions, will have half-metallic interfaces and coherent tunneling conductance through the $\Delta_1$ channel.

## IV. SUMMARY

In this paper, we have studied electronic and transport properties of MTJs with $Co_2YZ(YZ=MnSi,CrAl)$ and MgO barrier on the basis of the first-principles density-functional calculations. The results show that the $YZ$ terminations of the $Co_2YZ/MgO(001)$ junctions are thermodynamically stable as compared with the Co terminations as a result of relaxation of atomic positions in the $YZ$-terminated interfaces. In particular, the CrAl-terminated $Co_2CrAl/MgO(001)$ interface is half metallic in both sides of the junctions, while the MnSi-terminated $Co_2MnSi/MgO(001)$ interface looses the half metallicity of $Co_2MnSi$. We have concluded that the charge transfer from minority- to majority-spin states in Cr $3d_\epsilon$ plays an important role to make the half-metallic gap in the CrAl-terminated $Co_2CrAl/MgO$ junction. Furthermore, conductance of the $Co_2CrA/MgO/Co_2CrAl$ (001) MTJ is much smaller than that of the $Co_2MnSi/MgO/Co_2MnSi$ (001) MTJ in the parallel magnetization. Transport properties of $Co_2YZ/MgO/Co_2YZ$ (001) MTJs are explained by the electronic structure of bulk $Co_2YZ$ along [001], i.e., the position of the $\Delta_1$ band relative to the Fermi energy, which changes according to the number of valence electrons. On the basis of these results, we have proposed that addition of an ultrathin $Co_2CrAl$ layer between $Co_2MnSi$ electrode and MgO barrier, i.e., $Co_2MnSi/Co_2CrAl/MgO(001)$ junction, is effective to eliminate interface states in both sides of the junction while preserving the coherent tunneling through the $\Delta_1$ channel of the MTJ in the parallel magnetization. Finally, we have generalized our proposal to $Co_2YZ(Z_v \geq 28)/Co_2YZ(Z_v \approx 27)/MgO(001)$ junctions. All these findings suggest that half-metallic character at interfaces and transport properties of MTJs with MgO and $Co_2YZ$ can be designed by controlling their junctions, and that is worth further investigations.

## ACKNOWLEDGMENTS

This work was supported in part by a Grant-in-Aid for Scientific Research in Priority Areas, "Creation and Control of Spin Current" (Contract No. 19048002) and "Development of New Quantum Simulators and Design" (Contract No. 17064001), and by "High-Performance Low-Power Consumption Spin Devices and Storage Systems" program under Research and Development for Next-Generation Information Technology by MEXT.

[1] T. Miyazaki and N. Tezuka, J. Magn. Magn. Mater. **139**, L231 (1995).
[2] J. S. Moodera, L. R. Kinder, T. M. Wong, and R. Meservey, Phys. Rev. Lett. **74**, 3273 (1995).
[3] R. A. de Groot, F. M. Mueller, P. G. van Engen, and K. H. J. Buschow, Phys. Rev. Lett. **50**, 2024 (1983).
[4] K. Schwarz, J. Phys. F: Met. Phys. **16**, L211 (1986).
[5] W. E. Pickett and D. J. Singh, Phys. Rev. B **53**, 1146 (1996).
[6] S. Ishida, S. Fujii, S. Kashiwagi, and S. Asano, J. Phys. Soc. Jpn. **64**, 2152 (1995).
[7] S. Picozzi, A. Continenza, and A. J. Freeman, Phys. Rev. B **66**, 094421 (2002).
[8] I. Galanakis, P. H. Dederichs, and N. Papanikolaou, Phys. Rev. B **66**, 174429 (2002).
[9] M. Shirai, Physica E (Amsterdam) **10**, 143 (2001); J. Appl. Phys. **93**, 6844 (2003).
[10] J. G. Booth, in *Ferromagnetic Materials*, edited by E. P. Wohlfarth and K. H. J. Buschow (Elsevier Science, Amsterdam, 1988), Vol. 4, p. 288.
[11] Y. Miura, K. Nagao, and M. Shirai, Phys. Rev. B **69**, 144413 (2004); Y. Miura, M. Shirai, and K. Nagao, J. Appl. Phys. **95**, 7225 (2004).
[12] Y. Miura, M. Shirai, and K. Nagao, J. Appl. Phys. **99**, 08J112 (2006).
[13] K. Inomata, S. Okamura, R. Goto, and N. Tezuka, Jpn. J. Appl. Phys., Part 2 **42**, L419 (2003).
[14] H. Kubota, J. Nakata, M. Oogane, Y. Ando, A. Sakuma, and T. Miyazaki, Jpn. J. Appl. Phys., Part 2 **43**, L984 (2004).
[15] S. Okamura, A. Miyazaki, S. Sugimoto, N. Tezuka, and K. Inomata, Appl. Phys. Lett. **86**, 232503 (2005).
[16] Y. Sakuraba, M. Hattori, M. Oogane, Y. Ando, H. Kato, A. Sakuma, T. Miyazaki, and H. Kubota, Appl. Phys. Lett. **88**, 192508 (2006).
[17] N. Tezuka, N. Ikeda, A. Miyazaki, S. Sugimoto, M. Kikuchi, and K. Inomata, Appl. Phys. Lett. **89**, 112514 (2006).
[18] W. H. Butler, X.-G. Zhang, T. C. Schulthess, and J. M. MacLaren, Phys. Rev. B **63**, 054416 (2001).
[19] J. Mathon and A. Umerski, Phys. Rev. B **63**, 220403(R) (2001).
[20] S. Yuasa, T. Nagahama, A. Fukushima, Y. Suzuki, and K. Ando, Nat. Mater. **3**, 868 (2004).
[21] S. S. P. Parkin, C. Kaiser, A. Panchula, P. M. Rice, B. Hughes, M. Samant, and S.-H. Yang, Nat. Mater. **3**, 862 (2004).
[22] S. Ikeda, J. Hayakawa, Y. M. Lee, F. Matsukura, Y. Ohno, T. Hanyu, and H. Ohno, IEEE Trans. Electron Devices **54**, 991 (2007).
[23] N. Tezuka, N. Ikeda, S. Sugimoto, and K. Inomata, Appl. Phys. Lett. **89**, 252508 (2006).
[24] T. Marukame and M. Yamamoto, J. Appl. Phys. **101**, 083906 (2007).
[25] T. Ishikawa, S. Hakamata, K.-i. Matsuda, T. Uemura, and M. Yamamoto, J. Appl. Phys. **103**, 07A919 (2008).
[26] M. Lezaic, P. Mavropoulos, J. Enkovaara, G. Bihlmayer, and S. Blügel, Phys. Rev. Lett. **97**, 026404 (2006).
[27] L. Chioncel, Y. Sakuraba, E. Arrigoni, M. I. Katsnelson, M. Oogane, Y. Ando, T. Miyazaki, E. Burzo, and A. I. Lichtenstein, Phys. Rev. Lett. **100**, 086402 (2008); M. I. Katsnelson, V. Yu. Irkhin, L. Chioncel, A. I. Lichtenstein, and R. A. de Groot, Rev. Mod. Phys. **80**, 315 (2008).
[28] P. Mavropoulos, M. Lezaic, and S. Blügel, Phys. Rev. B **72**, 174428 (2005).
[29] J. P. Perdew, K. Burke, and M. Ernzerhof, Phys. Rev. Lett. **77**, 3865 (1996).
[30] S. Baroni, A. Dal Corso, S. de Gironcoli, and P. Giannozzi, http://www.pwscf.org
[31] H. Joon Choi and J. Ihm, Phys. Rev. B **59**, 2267 (1999).
[32] A. Smogunov, A. Dal Corso, and E. Tosatti, Phys. Rev. B **70**, 045417 (2004).
[33] S. J. Hashemifar, P. Kratzer, and M. Scheffler, Phys. Rev. Lett. **94**, 096402 (2005).
[34] Y. Miura, H. Uchida, Y. Oba, K. Nagao, and M. Shirai, J. Phys.: Condens. Matter **19**, 365228 (2007).
[35] I. Galanakis, J. Phys.: Condens. Matter **14**, 6329 (2002).
[36] K. Nagao, Y. Miura, and M. Shirai, Phys. Rev. B **73**, 104447 (2006); K. Nagao, M. Shirai, and Y. Miura, J. Phys.: Condens. Matter **16**, S5725 (2004).
[37] O. Wunnicke, N. Papanikolaou, R. Zeller, P. H. Dederichs, V. Drchal, and J. Kudrnovsky, Phys. Rev. B **65**, 064425 (2002).
[38] K. Kobayashi, R. Y. Umetsu, R. Kainuma, K. Ishida, T. Oyamada, R. Kainuma, K. Ishida, R. Y. Umetsu, A. Fujita, and K. Fukamichi, Appl. Phys. Lett. **85**, 4684 (2004).
[39] S. Kawagishi, T. Uemura, Y. Imai, K.-i. Matsuda, and M. Yamamoto, J. Appl. Phys. **103**, 07A703 (2008).